

Fluctuation Spectrum of 2+1D Critical Fermi Surface and its Application to Optical Conductivity and Hydrodynamics

Haoyu Guo

*Laboratory of Atomic and Solid State Physics, Cornell University,
142 Sciences Drive, Ithaca NY 14853-2501, USA*

(Dated: November 9, 2023)

We extend the kinetic operator formalism developed in the companion paper [H.Guo,arXiv:2311.03455] to study the general eigenvalues of the fluctuation normal modes. We apply the formalism to calculate the optical conductivity of a critical Fermi surface near the Ising-Nematic quantum critical point. We find that the conductivity is the sum of multiple conduction channels including both the soft and non-soft eigenvectors of the kinetic operator, and therefore it is not appropriate to interpret the optical conductivity using extended Drude formula for momentum conserved systems. We also show that the propagation of the FS soft modes is governed by a Boltzmann equation from which hydrodynamics emerges. We calculate the viscosity and it shows clear signature of the non-Fermi liquid physics.

CONTENTS

I. Introduction	1
II. The Fluctuation Spectrum of the 2+1D critical FS	3
A. The NFL regime (A) and the perturbative NFL regime (B)	5
B. The FL regime with small-angle scattering (C)	6
C. The FL regime with large-angle scattering (D)	6
III. Optical Conductivity	6
A. Circular FS with non-Parabolic Dispersion	7
B. Non circular FS	8
IV. Hydrodynamics	8
A. Derivation of a Boltzmann equation for the soft modes	9
B. Conventional Hydrodynamics Regime	11
C. Tomographic Regime	11
V. Conclusion	12
Acknowledgments	13
References	13

particular, this model is believed to describe the non-Fermi liquid (NFL) state, where the strong fermion-boson coupling destroys the coherent fermionic quasiparticles. Starting from the seminal work by Sung-Sik Lee [8], various large- N approaches have been proposed to analytically control the problem including dimensional/codimensional regularizations of the FS or deforming the boson dispersion (see [1] for review), or theories inspired by the Sachdev-Ye-Kitaev model that utilized random coupling in flavor space [43–45, 51, 52, 54, 55]. While these large- N theories differ in detail, their leading order behavior conforms to the Migdal-Eliashberg framework [56], where the vertex correction of the Yukawa coupling is ignored in the computation of the self-energies of the fermion and the boson.

In this paper we study the transport properties of a translational invariant critical Fermi surface in 2+1 spacetime dimensions. The uniform conductivity $\sigma(\omega)$ is heavily constrained by momentum conservation. First, because of the nonzero overlap between the current and the momentum, the DC conductivity σ_{DC} diverges (we ignore umklapp effects). Second, the finite-frequency optical conductivity $\sigma(\omega)$ is constrained by statements like Kohn's theorem [57]. In particular, the proposed $|\omega|^{-2/3}$ correction [6] to the Drude conductivity is cancelled for a Galilean invariant band structure [44, 51, 58, 59] and the scaling of the next order term is not settled. Another issue is the appropriateness of the extended Drude model [60–62] for optical conductivity. While it is always mathematically correct to parameterize $\sigma(\omega)$ with a frequency-dependent effective mass $m(\omega)/m$ and scattering rate $1/\tau(\omega)$, the physical picture implied in this parameterization is that the dissipations are related to the Drude peak, which is related to the physics of momentum dissipation. This interpretation is not compatible with a translational invariant system where momentum is conserved.

Part of the goals of this paper is to provide an answer

I. INTRODUCTION

The critical Fermi surface model of a Fermi surface (FS) coupled to a gapless bosonic field is a toy model for various finite-density quantum matter [1–53]. In

for the questions raised above. We utilize the formalism developed in the companion paper [63], where we obtained the fluctuation spectrum of a 2+1D critical FS by diagonalizing the Bethe-Salpeter kernel K_{BS} within the Migdal-Eliashberg theory. The optical conductivity can then be evaluated in a spectral decomposition fashion by projecting the current operator onto eigenmodes of K_{BS} . The optical conductivity we obtained can be written as the sum of various conduction channels and only one of them is the Drude peak, in contrast with the extended Drude model. When the band structure is Galilean invariant (i.e. parabolic), only the Drude peak contribution survives and we recover $\sigma(\omega) = ne^2/(-i\omega m)$. When the band is not Galilean invariant, there will be contributions from other channels and also corrections to the Drude peak. The conduction channels can be roughly classified into two types. The first type has nonzero overlap with the current at zero energy, which includes the momentum channel yielding the Drude peak and odd-parity deformations of the FS which has a slow relaxation rate [63]. The second type are operators that only overlap with the current at finite energy and they produce an incoherent contribution to the conductivity.

While the uniform conductivity is dominated by the Drude peak where the critical FS physics only enters as a correction, the non-local conductivity $\sigma(\mathbf{p})$ is a more informing quantity that reflects the critical FS physics. This is because momentum conservation facilitates the emergence of hydrodynamic transport [64–81]. Another goal of this paper is to provide a description of the hydrodynamic transport of the critical FS. At the longest length scale, the fermion-boson fluid is described by the Navier-Stokes equation with a viscosity term ν and we demonstrate that this viscosity is directly related to the soft eigenvalue λ_2 of K_{BS} which is derived in the companion paper [63]. Because K_{BS} contains a large number of soft modes, at an intermediate length scale $L < L_{\text{tom}}$ all these soft modes propagate collectively in space and the system enters the tomographic transport regime [82, 83]. This regime is characterized by a scale-dependent viscosity $\nu(\mathbf{p})$ and its scaling property is a non-perturbative synthesis of the soft mode eigenvalues λ_m .

To be concrete, we will use the model of a fermion ψ coupled to a real scalar boson ϕ with Yukawa coupling g , which describes the Ising-Nematic quantum critical point (QCP):

$$\mathcal{L} = \psi^\dagger(\partial_\tau + \hat{\varepsilon}_k)\psi + \frac{1}{2}\phi(\hat{q}^2 + r)\phi + g\psi^\dagger\psi\phi. \quad (1.1)$$

Here $\hat{\varepsilon}_k$ and \hat{q}^2 are differential operators that correspond to the dispersion. We work in the unit where boson velocity $v_B = 1$. The bare ∂_τ^2 dynamics of the boson term is dropped because it is irrelevant compared to the generated Landau damping. Our calculation is not sensitive

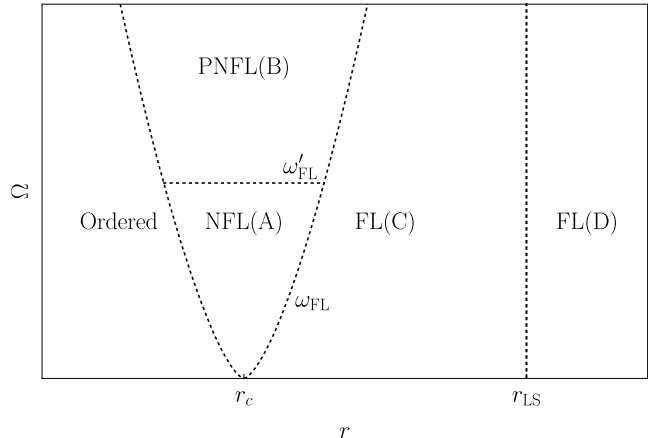


FIG. 1: Phase diagram near the Ising-nematic quantum critical point in terms of external frequency Ω and the tuning parameter r . The quantum critical point corresponds to $m_b^2 = r - r_c = 0$. When $r < r_c$ the system orders at $T = 0$. The regimes of interest are labelled A,B,C,D. A is the quantum critical NFL regime with $z = 3$ boson. B is a perturbative NFL (PNFL) regime where the boson still has $z = 3$ but the fermion self energy $\Sigma(i\omega)$ is small compared to ω . C is a Fermi liquid regime where the boson ϕ acquires a mass term $0 < m_b \ll k_F$. D is a Fermi liquid regime where the boson mass $m_b \gtrsim k_F$.

to the form factor of the Yukawa coupling, and we have set it to one for simplicity. The theory (1.1) will be handled using the Migdal-Eliashberg framework, which can be formally justified by the Yukawa-SYK model [35, 43, 44, 51, 52] or the small- $(z_b - 2)$ -large- N expansion [10]. We will use r as a tuning parameter to access different regimes of the system as shown in Fig. 1. The QCP is reached when $r = r_c$ and the boson is massless. Regime A is the NFL regime where the boson has dynamical exponent $z = 3$ and the fermion self-energy is $\Sigma(i\omega) \propto \omega^{2/3} \gg \omega$. Regime B is the perturbative NFL (PNFL) regime where the scaling is the same as regime A but $\Sigma(i\omega) \ll \omega$. Regime C is the FL regime where the boson becomes massive with mass $m_b^2 = r - r_c$. In regime C $m_b \ll k_F$ so the boson still mediates small-angle scattering. Regime D is also the FL regime but the boson mass m_b becomes comparable to k_F so the boson mediates large-angle scattering. Explicit calculations will be performed for regions A,B,C and qualitative results will be presented for regime D. We also note that in [63] we showed that the Eliashberg theory is unstable in the NFL regime (A), but in this paper we will nevertheless calculate its transport properties and ignore the instability. We will perform calculations at $T = 0$ and ignore the thermal fluctuations to extrapolate Ω scalings to finite T to obtain scalings in T .

The plan of the paper is as follows. In Sec. II we will

review the fluctuation spectrum of the 2+1D critical FS which is discussed in the companion paper [63]. In particular, we will extend the analysis in [63] to calculate the non-soft eigenvalues which is crucial for optical conductivity. In Sec. III we apply the formalism to calculate the optical conductivity. In Sec. IV, we apply the formalism to hydrodynamics and compute the viscosity.

II. THE FLUCTUATION SPECTRUM OF THE 2+1D CRITICAL FS

In this section, we briefly review the formalism developed in the companion paper [63]. In [63] we mainly focused on the soft modes and here extend it to study the nonzero eigenvalues. Within the Migdal-Eliashberg theory, the Schwinger-Dyson equations for the theory (1.1) is given by a set of translational invariant solutions $G(x_1, x_2) = G(x_1 - x_2)$, $D(x_1, x_2) = D(x_1 - x_2)$ where G and D are the fermion and the boson Green's functions respectively, given by:

$$\begin{aligned} G(i\omega, \mathbf{k}) &= \frac{1}{i\omega - \xi_{\mathbf{k}} - \Sigma(i\omega, \mathbf{k})}, \\ D(i\Omega, \mathbf{q}) &= \frac{1}{|\mathbf{q}|^2 + m_b^2 - \Pi(i\Omega, \mathbf{q})}, \\ \Sigma(\tau, \mathbf{r}) &= g^2 G(\tau, \mathbf{r}) D(\tau, \mathbf{r}), \\ \Pi(\tau, \mathbf{r}) &= -g^2 G(\tau, \mathbf{r}) G(-\tau, -\mathbf{r}). \end{aligned} \quad (2.1)$$

The object we study is the Bethe-Salpeter kernel K_{BS} , which can be defined through the bilinear fluctuation around the saddle point (2.1):

$$S[\delta G] = \frac{1}{2} \int_{x_1, x_2, x_3, x_4} \delta G(x_2, x_1) K_{\text{BS}}(x_1, x_2; x_3, x_4) \delta G(x_3, x_4). \quad (2.2)$$

Here $\delta G(x_1, x_2)$ is the fluctuation of the fermion bilinear $-T_\tau \langle \psi(x_1) \psi^\dagger(x_2) \rangle$ around the SD equation solution (2.1). Here x_1, x_2 etc. denote spacetime indices. The utility of K_{BS} is to compute the linear response of fermion bilinears. For example, given two operators $\hat{A} = \int_{x_1, x_2} A(x_1, x_2) \psi^\dagger(x_1) \psi(x_2)$ and $\hat{B} = \int_{x_3, x_4} B(x_3, x_4) \psi^\dagger(x_3) \psi(x_4)$, we have

$$\langle \hat{A} \hat{B} \rangle = \int_{x_1, x_2, x_3, x_4} A(x_2, x_1) K_{\text{BS}}^{-1}(x_1, x_2; x_3, x_4) B(x_3, x_4). \quad (2.3)$$

As we will see, an efficient way to evaluate this functional inverse is to use its spectral decomposition.

From (2.2), we see that K_{BS} is a functional that acts on two-point functions. It is also convenient to fourier transform two-point functions in real space to momentum space using the center-of-mass (CoM) and relative

3-momenta,

$$\begin{aligned} F(\mathbf{k}; p) &= \int d^3 x_1 d^3 x_2 F(x_1, x_2) \\ &\times \exp(-ip \cdot (x_1 + x_2)/2 - ik \cdot (x_1 - x_2)). \end{aligned} \quad (2.4)$$

Because of translational symmetry, p is conserved by K_{BS} . In this section we will work in the homogeneous limit $p = (i\Omega, 0)$ and the retarded branch $\Omega > 0$. For notational clarity we will suppress p in $F(\mathbf{k}; p)$ unless otherwise mentioned.

As discussed in [63], the correct operator to diagonalize is the kinetic operator L :

$$L = K_{\text{BS}} \circ M - \Omega I, \quad (2.5)$$

where I is the identity operator and M is a functional whose action in the momentum space is diagonal:

$$M[F](i\omega, \mathbf{k}) = (iG(i\omega + i\Omega/2, \mathbf{k}) - iG(i\omega - i\Omega/2, \mathbf{k})) F(i\omega, \mathbf{k}). \quad (2.6)$$

The kinetic operator L is symmetric under the following inner product:

$$\begin{aligned} \langle A|B \rangle &= \int \frac{d\omega d^2 \mathbf{k}}{(2\pi)^3} A(i\omega, \mathbf{k}) \\ &\times (iG(i\omega + i\Omega/2, \mathbf{k}) - iG(i\omega - i\Omega/2, \mathbf{k})) B(i\omega, \mathbf{k}). \end{aligned} \quad (2.7)$$

From now on we assume the Fermi surface is circular, and we utilize the rotation symmetry to consider L restricted to angular harmonics number m i.e. $F(\mathbf{k}) = F(i\omega, \xi_{\mathbf{k}}) e^{im\theta_{\mathbf{k}}}$. The kinetic operator L can be diagrammatically represented as the sum of density-of-states, Maki-Thompson and Aslamazov-Larkin diagrams. In [63], it is shown that L_m can be handled using a double expansion in the dispersion ξ and the boson momentum $|\mathbf{q}|$:

$$\begin{aligned} L_m &= L_m^{(0)} + L_m^{(1)} + L_m^{(2)} + \dots \\ &\quad \parallel \quad \parallel \quad \parallel \\ &\delta_q^0 L_m^{(0)} \quad \delta_q^0 L_m^{(1)} \quad \delta_q^0 L_m^{(2)} \\ &+ \quad + \quad + \\ &\delta_q^1 L_m^{(0)} \quad \delta_q^1 L_m^{(1)} \quad \delta_q^1 L_m^{(2)} \\ &+ \quad + \quad + \\ &\vdots \quad \vdots \quad \vdots \end{aligned} \quad (2.8)$$

Here the horizontal direction corresponds to the $\xi/(k_F v_F)$ expansion and the vertical direction corresponds to the $|\mathbf{q}|/k_F$ expansion. In the large k_F limit, the eigenvalues of L_m are dominated by the leading order term $\delta_q^0 L_m^{(0)}$ which describes the forward scattering limit due to shape fluctuations of the FS. The exception is when zero modes occur and the effects of the

higher order terms leads to be taken into account seriously, which has been done in [63]. Here we are instead interested in the nonzero eigenvalues so it is sufficient

$$\begin{aligned} \delta_q^0 L_{\text{MT+DOS},m}^{(0)}[F](i\omega, \xi) &= g^2 \int_{-\infty}^{\infty} \frac{d\omega'}{2\pi} \frac{\mathcal{N}d\xi'}{2\pi} \int \frac{d|\mathbf{q}|}{k_F} D(|\mathbf{q}|, i\omega - i\omega') \\ &\times 2 [iG(i\omega' + i\Omega/2, \xi') - iG(i\omega' - i\Omega/2, \xi')] [F(i\omega, \xi) - F(i\omega', \xi')]. \end{aligned} \quad (2.9)$$

$$\begin{aligned} \delta_q^0 L_{\text{AL},m}^{(0)}[F](i\omega_1, \xi_1) &= -g^4 (2\pi)^2 (1 + (-1)^m) \mathcal{N}^3 \text{sgn} \omega_1 \int_{-\infty}^{\infty} \frac{d\nu}{2\pi} \frac{d\omega_2}{2\pi} \frac{d\xi_2}{2\pi} \int_0^{\infty} \frac{d|\mathbf{q}|}{k_F^2 |\mathbf{q}|} \\ &\times D(|\mathbf{q}|, i\nu + i\Omega/2) D(|\mathbf{q}|, i\nu - i\Omega/2) \text{sgn} \omega_2 \theta(|\omega_1| - |\nu|) \theta(|\omega_2| - |\nu|) \\ &\times i(G(i\omega_2 + i\Omega/2, \xi_2) - G(i\omega_2 - i\Omega/2, \xi_2)) F(i\omega_2, \xi_2). \end{aligned} \quad (2.10)$$

Here $\mathcal{N} = k_F/(2\pi v_F)$ is the density of states near the FS.

It will be convenient to write the function F in a polynomial basis in ξ , as the following

$$F(i\omega, \xi) = F_0(i\omega) + \frac{\xi}{A(i\Omega)} F_1(i\omega) + \left(\frac{\xi}{A(i\Omega)}\right)^2 F_2(i\omega) + \dots \quad (2.11)$$

Here $A(i\Omega) = i\Omega - \Sigma(i\Omega)$. The normalization ξ by $A(i\Omega)$ makes the matrix element of L_m of the equal scaling when acted on different powers of ξ . The hidden assumption of using the ansatz (2.11) is that we are interested in smooth function of ξ , which is satisfied by the physical observables such as density or current. We will use the notation \mathcal{H}_n to denote the Hilbert space of

to only consider $\delta_q^0 L_m^{(0)}$. The expression for L_m in this limit is given by the sum of the following

n -th monomial in ξ .

The structure of $\delta_q^{(0)} L_m^{(0)}$ is fairly simple. In Eq.(2.9) the term proportional to $F(i\omega, \xi)$ is diagonal in the $(i\omega, \xi)$ domain, and in the rest of (2.9) and (2.10) the result of the integral is independent of ξ . Therefore $\delta_q^{(0)} L_m^{(0)}$ has the following uppertriangular structure when written as blocks in \mathcal{H}_n :

$$\delta_q^0 L_m^{(0)} = \begin{pmatrix} \delta_q^0 L_m^{(0)}|_{\mathcal{H}_0} & \star & \star & & \\ 0 & \delta_q^0 L_m^{(0)}|_{\mathcal{H}_1} & 0 & \dots & \\ 0 & 0 & \delta_q^0 L_m^{(0)}|_{\mathcal{H}_2} & & \\ & \vdots & & \ddots & \end{pmatrix}. \quad (2.12)$$

The diagonal blocks with $n \geq 1$ has the form

$$\begin{aligned} \delta_q^0 L_m^{(0)}|_{\mathcal{H}_{n \geq 1}} [F](i\omega, \xi) &= g^2 F(i\omega, \xi) \int_{-\infty}^{\infty} \frac{d\omega'}{2\pi} \frac{\mathcal{N}d\xi'}{2\pi} \int \frac{d|\mathbf{q}|}{k_F} D(|\mathbf{q}|, i\omega - i\omega') \times 2 [iG(i\omega' + i\Omega/2, \xi') - iG(i\omega' - i\Omega/2, \xi')] \\ &= \underbrace{[i\Sigma(i\omega + i\Omega/2) - i\Sigma(i\omega - i\Omega/2)]}_{\Lambda_\omega} F(i\omega, \xi). \end{aligned} \quad (2.13)$$

Here in the second line we have used the Eliashberg equations (2.1) to evaluate the integral. This implies all eigenvalues of the $n \geq 1$ blocks are labelled by Λ_ω as defined in (2.13).

The remaining problem is to obtain the eigenvalues of the zeroth block $\delta_q^0 L_m^{(0)}|_{\mathcal{H}_0}$. In this block the $F = F(i\omega)$ is a function of frequency only. From now on we will need to know the details of the system in different

regimes.

A. The NFL regime (A) and the perturbative NFL regime (B)

In the NFL (A) and PNFL (B) regimes, the solution of Eq.(2.1) is given by [44]

$$\Sigma(i\omega) = -ic_f|\omega|^{2/3}\text{sgn}\omega, \quad c_f = \frac{g^2}{2\sqrt{3}\pi v_F \gamma^{1/3}}, \quad (2.14)$$

$$D(i\Omega, \mathbf{q}) = \frac{1}{|\mathbf{q}|^2 + \gamma|\Omega|/|\mathbf{q}|}, \quad \gamma = \frac{\mathcal{N}g^2}{v_F}. \quad (2.15)$$

Using this to evaluate the $|\mathbf{q}|$ integrals in Eqs.(2.9) and (2.10), we obtain

$$\delta_q^0 L_{\text{MT+DOS},m}^{(0)}[F](i\omega) = \frac{2}{3}c_f \int_{-\Omega/2}^{\Omega/2} d\omega' \frac{1}{|\omega - \omega'|^{1/3}} [F(i\omega) - F(i\omega')]. \quad (2.16)$$

$$\begin{aligned} \delta_q^0 L_{\text{AL},m}^{(0)}[F](i\omega_1) &= -\frac{2}{3}c_f \text{sgn}\omega_1 \frac{1 + (-1)^m}{2} \int_{-\Omega/2}^{\Omega/2} d\omega_2 \int_{-\Omega/2}^{\Omega/2} d\nu \theta(|\omega_1| - |\nu|) \theta(|\omega_2| - |\nu|) \\ &\times \frac{1}{|\nu^2 - \Omega^2/4|^{1/3} (|\nu + \Omega/2|^{2/3} + |\nu - \Omega/2|^{2/3} + |\nu^2 - \Omega^2/4|^{1/3})} \text{sgn}\omega_2 F(i\omega_2). \end{aligned} \quad (2.17)$$

P	$(-1)^m$	Discrete Spectrum	Continuum Spectrum
1	1	$\alpha = 0$	$\alpha \in [1.386, 1.890]$
	-1		
-1	1	$\alpha = 0.856, 1.411, 1.484$	$\alpha \in [1.498, 1.890]$
	-1	$\alpha = 1.226, 1.449, 1.491$	$\alpha \in [1.499, 1.890]$

TABLE I: Spectrum of $\delta_q^0 L_m^{(0)} \Big|_{\mathcal{H}_0}$ in regimes A and B in different sectors defined by P and $(-1)^m$. Numerical values are obtained through a 5000 by 5000 discretization of Eqs.(2.16) and (2.17).

Because of the ξ -integral the range of ω has been bounded to $[-\Omega/2, \Omega/2]$. We observe that Eqs.(2.16) and (2.17) has a particle-hole symmetry $F(i\omega) \rightarrow F(-i\omega)$, implying that the eigenvalues can be considered separately for odd and even sectors, i.e. $F(-i\omega) = PF(i\omega)$, $P = \pm 1$. It is easy to diagonalize (2.16) and (2.17) numerically, the result can be written as

$$\lambda_\alpha^m = \frac{2}{3}c_f \Omega^{2/3} \alpha, \quad (2.18)$$

where α is a dimensionless factor. Our numerical result is summarized in Table. I.

For the $P = 1$ sector, we found a zero mode which

$(-1)^m$	Discrete Spectrum	Continuum Spectrum
1	$\alpha = 0.856$	$\alpha \in [1.386, 1.890]$
-1	$\alpha = 1.226$	$\alpha \in [1.386, 1.890]$

TABLE II: The approximate non-soft spectrum of L_m in regimes A and B after breaking particle-hole symmetry.

is studied in detail in the companion paper [63]. Apart from that, we found a continuum spectrum with $\alpha \in [1.386, 1.890]$. In the $P = -1$ sector, we also found 3 discrete modes together with a continuum as shown in Table. I.

However, the particle-hole symmetry only holds for the leading order term $L_m^{(0)}$. Generically $L_m^{(n)}$ has signature $(-1)^n$ under particle-hole transformation $(\omega, \xi) \rightarrow (-\omega, -\xi)$, so the symmetry is broken for L_m . Therefore, after putting back the higher perturbations $P = \pm 1$ modes will hybridize and the spectra merge into one, with some discrete modes buried into the continuum. So the correct approximate spectrum should be given by Table. II.

	$(-1)^m$	Discrete			Continuum
(A_α, B_α)	1	(0.995,0.981)	(2.000,1.407)	(0.998,0.994)	Fig. 2
	-1	(0.995,0.981)	(1.219,1.076)	(0.999,0.999)	

TABLE III: The approximate spectrum of L_m in regime C. The first discrete mode is approximately even and the other two modes are approximately odd under particle-hole symmetry.

B. The FL regime with small-angle scattering (C)

The boson propagator is

$$D(i\Omega, \mathbf{q}) = \frac{1}{|\mathbf{q}|^2 + m_b^2 + \gamma|\Omega|/|\mathbf{q}|}. \quad (2.19)$$

The FL regime is characterized by the condition that the Landau damping only enters perturbatively, with the criterion $|\Omega| \ll \omega_{\text{FL}} = m_b^3/\gamma$. The fermion self-

energy is then evaluated perturbatively in $1/m_b$, with the result

$$\Sigma(i\omega) = (-i\omega)c'_f \left(\pi + \frac{|\omega|}{\omega_{\text{FL}}} \ln \left(\frac{|\omega|}{\omega_{\text{FL}}} \right) \right), \quad (2.20)$$

where $c'_f = g^2 \mathcal{N}/(2\pi k_F m_b)$.

With this information, we can again perform the q -integral in (2.9) and (2.10) to obtain

$$\delta_q^0 L_{\text{MT+DOS},m}^{(0)}[F](i\omega) = c'_f \int_{-\Omega/2}^{\Omega/2} d\omega' \left(\pi + \frac{2|\omega - \omega'|}{\omega_{\text{FL}}} \ln \left(\frac{|\omega - \omega'|}{\omega_{\text{FL}}} \sqrt{e} \right) \right) (F(i\omega) - F(i\omega')), \quad (2.21)$$

$$\begin{aligned} \delta_q^0 L_{\text{AL},m}^{(0)}[F](i\omega) &= 2 \frac{c'_f}{\omega_{\text{FL}}} \frac{1 + (-1)^m}{2} \int_{-\Omega/2}^{\Omega/2} d\nu \int_{-\Omega/2}^{\Omega/2} d\omega_2 \text{sgn} \omega_1 \theta(|\omega_1| - |\nu|) \theta(|\omega_2| - |\nu|) \\ &\frac{|\nu + \Omega/2| \ln \left(\frac{\gamma|\nu + \Omega/2|}{m_b^3} \sqrt{e} \right) - |\nu - \Omega/2| \ln \left(\frac{\gamma|\nu - \Omega/2|}{m_b^3} \sqrt{e} \right)}{|\nu + \Omega/2| - |\nu - \Omega/2|} \text{sgn} \omega_2 F(\omega_2). \end{aligned} \quad (2.22)$$

Similar to the regimes A and B, we can numerically diagonalize Eqs. (2.21) and (2.22), and we found the result can be well fitted by the function

$$\lambda_\alpha = c'_f A_\alpha \frac{\Omega^2}{\omega_{\text{FL}}} \ln \left(\frac{B_\alpha \Omega}{\omega_{\text{FL}}} \right). \quad (2.23)$$

C. The FL regime with large-angle scattering (D)

In this regime, the form of the kinetic operator L_m is complicated because the boson momentum $|\mathbf{q}|$ can be as large as $2k_F$. Therefore, we do not have analytical control as we did in regimes A,B,C. However, from the analysis above we see that the nonzero eigenvalues of L_m is not suppressed compared to the self-energy scaling by the small-angle scattering. Therefore, we expect the nonzero eigenvalues of L_m should scale similarly as the self-energy and be qualitatively similar to regime C.

The parameters A_α and B_α are summarized in Table. III and Fig. 2. We found three discrete modes together with a continuum (the zero mode is already excluded). The parameters of the discrete modes are listed in Table. III and the continuum parameters are plotted in Fig. 2 as a function of $\alpha \in [0, 1]$.

III. OPTICAL CONDUCTIVITY

In this section, we apply the eigenvalues we obtained to calculate the optical conductivity at the homogeneous limit $\mathbf{q} = 0$. Rewriting the Kubo formula derived in [44], the optical conductivity before analytic continuation can be written as

$$\sigma(i\Omega) = \frac{2\pi e^2}{\Omega} \langle v_k | \frac{1}{L + \Omega} | v_k \rangle. \quad (3.1)$$

We can expand it using eigenvalues of L , and we obtain

$$\sigma(i\Omega) = \frac{2\pi e^2}{\Omega} \sum_i \frac{\langle v_k | i \rangle \langle i | v_k \rangle}{\Omega + \lambda_i}. \quad (3.2)$$

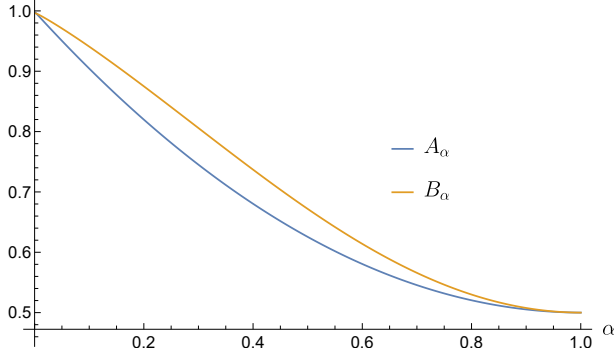


FIG. 2: The functions A_α and B_α parameterizing the continuum spectrum in regime C.

Therefore, we need to compute the overlap of velocity with the eigenfunctions using inner product (2.7). The details depend on the FS shape and dispersion, which we discuss below.

A. Circular FS with non-Parabolic Dispersion

We first consider a circular FS with non-Parabolic dispersion. We expand $|\mathbf{k}|$ as a function of ξ_k around the Fermi level:

$$|\mathbf{k}| = k_F + \frac{\xi_k}{v_F} - \frac{\kappa}{2} \frac{\xi_k^2}{k_F v_F^2} + \frac{\zeta}{2} \frac{\xi_k^3}{k_F^2 v_F^3} + \mathcal{O}(\xi_k^4). \quad (3.3)$$

κ and ζ are dimensionless numbers. In a Galilean invariant system, $\kappa = \zeta = 1$. The velocity is then

$$v_k = v_F + \frac{\kappa \xi_k}{k_F} + \frac{2\kappa^2 - 3\zeta}{2k_F^2 v_F} \xi_k^2. \quad (3.4)$$

We will perform calculation to order $\mathcal{O}(\xi_k^2)$.

With the rotation symmetry, we only need to consider eigenvectors of L_1 . L_1 contains a zero mode which is the momentum $|k\rangle$. We decompose the velocity $|v_k\rangle = |v_k^\parallel\rangle + |v_k^\perp\rangle$ which is the projection along the momentum and the orthogonal complement. The overlap between the velocity $|v_k\rangle$ and the momentum is

$$\frac{\langle v_k | k \rangle \langle k | v_k \rangle}{\langle k | k \rangle} = v_F^2 \langle 1 | 1 \rangle + \frac{2\kappa^2 + 2\kappa - 3\zeta - 1}{k_F^2} \langle \xi | \xi \rangle. \quad (3.5)$$

We note that at low-energy when $\langle \xi | \xi \rangle$ can be neglected, the overlap is one hundred percent. This is due to the circular geometry of the FS.

The orthogonal complement is

$$|v_k^\perp\rangle = |v_k\rangle - |k\rangle \frac{\langle k | v_k \rangle}{\langle k | k \rangle} \simeq (\kappa - 1) \frac{|\xi\rangle}{k_F}. \quad (3.6)$$

Because $|v_k^\perp\rangle \propto |\xi\rangle$, its eigenvalues are given simply by Λ_ω as defined in Eq.(2.13).

The optical conductivity can be decomposed into two parts

$$\sigma(\omega) = \sigma_D(\omega) + \sigma_i(\omega). \quad (3.7)$$

The Drude contribution σ_D is due to the projection of $|v_k\rangle$ along the momentum

$$\sigma_D(i\Omega) = \frac{e^2 \mathcal{N} v_F^2}{2} \frac{1}{\Omega} \left[1 + (2\kappa^2 + 2\kappa + 3\zeta - 1) \frac{\langle \xi | \xi \rangle / \langle 1 | 1 \rangle}{v_F^2 k_F^2} \right], \quad (3.8)$$

where

$$\frac{\langle \xi | \xi \rangle}{\langle 1 | 1 \rangle} = \frac{1}{\Omega} \int_{-\Omega/2}^{\Omega/2} d\omega \frac{A(i\omega + i\Omega/2)^2 + A(i\omega - i\Omega/2)^2}{2}. \quad (3.9)$$

We recall that $A(i\omega) = i\omega - \Sigma(i\omega)$.

The incoherent conductivity arises from the current that is orthogonal to the momentum, i.e. (3.6). We have

$$\begin{aligned} \sigma_i(i\Omega) &= \frac{e^2 \mathcal{N} v_F^2}{2} \left(\frac{\kappa - 1}{v_F k_F} \right)^2 \frac{1}{\Omega} \int_{-\Omega/2}^{\Omega/2} d\omega \int \frac{d\xi}{2\pi} \\ &\times \frac{(iG(i\omega + i\Omega/2, \xi) - iG(i\omega - i\Omega/2, \xi)) \xi^2}{\Omega + \Lambda_\omega} \\ &= \frac{e^2 \mathcal{N} v_F^2}{2} \left(\frac{\kappa - 1}{v_F k_F} \right)^2 \frac{1}{\Omega} \int_{-\Omega/2}^{\Omega/2} d\omega \\ &\times \frac{1}{2} \frac{A(i\omega + i\Omega/2)^2 + A(i\omega - i\Omega/2)^2}{\Omega + \Lambda_\omega}, \end{aligned} \quad (3.10)$$

We notice that in the Galilean invariant limit $\kappa = \zeta = 1$, all the correction terms vanish and we are left with the Drude result $\sigma(i\Omega) = e^2 \mathcal{N}^2 v_F^2 / (2\Omega)$.

Next we can evaluate Eqs.(3.8) and (3.10) in different regimes. We notice that in the NFL regime (A), $A(i\omega) \simeq -\Sigma(i\omega)$ is dominated by the self-energy and $\Lambda_\omega \gg \Omega$. In other regimes $A(i\omega) \simeq i\omega$ and $\Lambda_\omega \ll \Omega$. In the NFL (A) and the PNFL (B) regimes we neglect the effect of boson thermal mass and the assumed ω/T scaling.

Our results are summarized in Table. IV where the results have been continued to real time $i\Omega \rightarrow \omega + i0$.

For the Drude peak term σ_D , we find a correction to the Drude weight at low frequency. At high frequencies, the correction to Σ_D is purely imaginary in the PNFL and the FL regime, but there is a real component in the NFL regime.

The incoherent conductivity σ_i is nonzero in all four regimes. In the NFL regime A, the incoherent part shows ω/T scaling, but it is sub-leading to the Drude peak term. In the PNFL regime B and FL regimes C,D, because $\Sigma < \omega$ the resulting σ_i does not show ω/T scaling.

Regime	$\lambda_{\text{even } m}^{\text{soft}}$	$\lambda_{\text{odd } m}^{\text{soft}}$ (Convex FS)	$\lambda_{\text{odd } m}^{\text{soft}}$ (Concave FS)
A	$m^2(c_f\Omega^{2/3})^2/(k_F v_F)$	$m^2(m^2-1)^2(c_f\Omega^{2/3})^4/(k_F v_F)^3$	$m^2(c_f\Omega^{2/3})^2/(k_F v_F)$
B	$m^2(c_f\Omega^{2/3})^2/(k_F v_F)$	$m^2(m^2-1)^2(c_f\Omega^{2/3})^2\Omega^2/(k_F v_F)^3$	$m^2(c_f\Omega^{2/3})^2/(k_F v_F)$
C	$m^2 m_b^2 c_f' \Omega^2 / (k_F^2 \omega_{\text{FL}})$	$m^2(m^2-1)^2 m_b^2 c_f' \Omega^4 / (k_F^4 v_F^2 \omega_{\text{FL}})$	$m^2 m_b^2 c_f' \Omega^2 / (k_F^2 \omega_{\text{FL}})$
D	$c_f' \Omega^2 \ln m / \omega_{\text{FL}}$	$c_f' \Omega^4 m^4 \ln m / (k_F^2 v_F^2 \omega_{\text{FL}})$	$c_f' \Omega^2 \ln m / \omega_{\text{FL}}$

TABLE V: The dissipative part of the soft mode eigenvalues in different regimes at $T = 0$. m is the angular harmonic number of a circular FS, and should be interpreted as the eigenvalue of the angular Laplacian for a general FS. Regimes A,B,C are computed in the companion paper [63]. Regime D is from [84].

Regimes	NFL(A)	PNFL(B)	FL(C,D)
$\frac{\text{Re}\sigma_D(\omega \gg T)}{e^2 \mathcal{N}^2 v_F^2}$	$\frac{c_f^2 \omega ^{1/3}}{k_F^2 v_F^2}$	0	0
$\frac{\text{Re}\sigma_D(\omega \ll T)}{e^2 \mathcal{N}^2 v_F^2}$	$\frac{c_f^2 T^{4/3}}{k_F^2 v_F^2} \delta(\omega)$	$\frac{T^2}{k_F^2 v_F^2} \delta(\omega)$	$\frac{T^2}{k_F^2 v_F^2} \delta(\omega)$
$\frac{\text{Re}\sigma_i(\omega \gg T)}{e^2 \mathcal{N}^2 v_F^2}$	$\frac{c_f \omega ^{2/3}}{k_F^2 v_F^2}$	$\frac{c_f \omega ^{2/3}}{k_F^2 v_F^2}$	$\frac{c_f \omega ^2 \ln(\omega /\omega_{\text{FL}})}{\omega_{\text{FL}} k_F^2 v_F^2}$
$\frac{\text{Re}\sigma_i(\omega \ll T)}{e^2 \mathcal{N}^2 v_F^2}$	$\frac{c_f T^{2/3}}{k_F^2 v_F^2}$	$\frac{c_f T^{8/3}}{ \omega ^2 k_F^2 v_F^2}$	$\frac{c_f T^4 \ln(T/\omega_{\text{FL}})}{\omega_{\text{FL}} \omega ^2 k_F^2 v_F^2}$

TABLE IV: Corrections to the real part of the optical conductivity of a circular FS in different regimes. The zeroth order Drude peak $\sigma_D^{(0)}(\omega) = \pi e^2 \mathcal{N} v_F^2 \delta(\omega)/2$ is subtracted. The numerical prefactors are neglected.

B. Non circular FS

When the FS is not circular, the velocity $|v_k\rangle$ does not fully overlap with momentum $|k\rangle$ even at zero energy. We decompose it as

$$|v_k\rangle = |v_k^{\parallel}\rangle + |v_{k,\xi=0}^{\perp}\rangle + |v_{k,\xi}^{\perp}\rangle. \quad (3.11)$$

To summarize, the total optical conductivity is the sum of all three contributions

$$\sigma(\omega) = \sigma_D(\omega) + \sigma'_D(\omega) + \sigma_i(\omega). \quad (3.13)$$

Our results agree with the recent calculation [42] which calculated $\sigma(\omega)$ using perturbation theory in the FL regime and later extrapolated to the PNFL regime. The results in [42] for the circular and the convex FS map to our incoherent conductivity σ_i in regimes B and C. The results in [42] for the concave FS, map to the our

Here $|v_k^{\parallel}\rangle$ is still the projection along the momentum, but the orthogonal complement has been further decomposed into a ξ -independent part $|v_{k,\xi=0}^{\perp}\rangle$, and a ξ -dependent part $|v_{k,\xi}^{\perp}\rangle$.

Following this decomposition, $|v_k^{\parallel}\rangle$ and $|v_{k,\xi}^{\perp}\rangle$ still contributes to σ_D and σ_i respectively similar to the circular FS case, but the numerical prefactors are different because of different FS geometry.

The interesting new contribution is from $|v_{k,\xi=0}^{\perp}\rangle$, which overlaps with the old-parity soft modes studied in the companion paper [63] when the FS is not circular. It leads to a term that looks like a modified Drude peak

$$\sigma'_D(i\Omega) = e^2 \mathcal{N} v_F^2 \frac{1}{\Omega + \lambda_{\text{odd}}^{\text{soft}}}. \quad (3.12)$$

We summarize the result for the soft eigenvalues $\lambda_{\text{odd}}^{\text{soft}}$ in Table. V. The results for regimes A,B,C are calculated in the companion paper [63]. Regime D, which involves large-angle scattering, is not as analytically tractable as regimes A,B,C. However, since D is deep in the FL, we quote the result of Ref. [84] which calculated the soft mode eigenvalues using classical Boltzmann equation, and it agrees with qualitative arguments presented in [63].

Next, we apply the soft mode results in Table. V to Eq.(3.12), and the resulting $\sigma'_D(\omega)$ is summarized in Table. VI. We have assumed the absence of boson thermal mass and so the soft mode eigenvalues are assumed to satisfy ω/T scaling.

σ'_D term in regimes B and C. However, because the calculation in [42] assumes $\Sigma \ll \omega$, it was unable to access our regime A which is the true NFL regime.

IV. HYDRODYNAMICS

In this section, we discuss the implication of our formalism in hydrodynamics. In the hydrodynamic regime, the non-local quantities quickly relax through local collision and only zero modes or soft modes are left. These

	FS geometry	A	B	C	D
$\frac{\text{Re}\sigma'_D(\omega \gg T)}{e^2 \mathcal{N} v_F^2}$	Convex	$\frac{c_f^4 \omega ^{2/3}}{(k_F v_F)^3}$	$\frac{c_f^2 \omega ^{4/3}}{(k_F v_F)^3}$	$\frac{m_b^2 c_f \omega ^2}{k_F^2 k_F^2 v_F^2 \omega_{\text{FL}}}$	$\frac{c_f \omega ^2}{k_F^2 v_F^2 \omega_{\text{FL}}}$
$\frac{\text{Re}\sigma'_D(\omega \ll T)}{e^2 \mathcal{N} v_F^2}$		$\frac{c_f^4 T^{8/3}}{(k_F v_F)^3 \omega ^2}$	$\frac{c_f^2 T^{10/3}}{(k_F v_F)^3 \omega ^2}$	$\frac{m_b^2 c_f T^4}{k_F^2 k_F^2 v_F^2 \omega_{\text{FL}} \omega ^2}$	$\frac{c_f T^4}{k_F^2 v_F^2 \omega_{\text{FL}} \omega ^2}$
$\frac{\text{Re}\sigma'_D(\omega \gg T)}{e^2 \mathcal{N} v_F^2}$	Concave	$\frac{c_f^2}{k_F v_F \omega ^{2/3}}$	$\frac{c_f^2}{k_F v_F \omega ^{2/3}}$	$\frac{m_b^2 c_f}{k_F^2 \omega_{\text{FL}}}$	$\frac{c_f}{\omega_{\text{FL}}}$
$\frac{\text{Re}\sigma'_D(\omega \ll T)}{e^2 \mathcal{N} v_F^2}$		$\frac{c_f^2 T^{4/3}}{k_F v_F \omega ^2}$	$\frac{c_f^2 T^{4/3}}{k_F v_F \omega ^2}$	$\frac{m_b^2 c_f T^2}{k_F^2 \omega ^2 \omega_{\text{FL}}}$	$\frac{c_f T^2}{ \omega ^2 \omega_{\text{FL}}}$

TABLE VI: The new Drude-like contribution for non-circular FS in different regimes. We assumed ω/T scaling for the soft mode eigenvalues.

conserved and quasi-conserved quantities then can start propagating in space. As a result of this propagation, the current-field relation $\mathbf{j} = \sigma \mathbf{E}$ is no-longer given by a conductivity σ , but instead is described through the non-local conductivity $\sigma(\mathbf{p})$:

$$\sigma(\mathbf{p}) = \frac{ne^2}{2\pi \mathcal{N} |\mathbf{p}|^2 \nu(\mathbf{p})}. \quad (4.1)$$

Here n is the total fermion density, and $\nu(\mathbf{p})$ is the kinematic viscosity, which can be written as

$$\nu(\mathbf{q}) = \frac{n}{4\pi \mathcal{N}^2 \Gamma_2(\mathbf{p})}, \quad (4.2)$$

and $\Gamma_2(\mathbf{p})$ is the effective scattering rate. The wavevector \mathbf{p} should be understood as a typical wavevector of the external drive, such as inverse sample size.

A. Derivation of a Boltzmann equation for the soft modes

To capture the non-local conductivity $\sigma(\mathbf{p})$, we need to allow a finite CoM momentum in our formalism, i.e.

$p = (i\Omega, \mathbf{p})$. In this subsection, we discuss how a Boltzmann equation naturally emerges from the soft modes. Unless otherwise mentioned, we will work with the circular FS.

Since the soft modes can now propagate in space, the eigenvalues of the kinetic operator L or the Bethe-Salpeter kernel K_{BS} is no longer an intrinsic property of the critical FS because it depends on the real space geometry of system. However, it is still useful to consider the operator

$$\mathcal{L} = K_{\text{BS}} \circ M. \quad (4.3)$$

We expand $K_{\text{BS}} = W_{\Sigma}^{-1} - W_{\text{MT}} - W_{\text{AL}}$ into three sets of Feynmann diagram contributions [44, 63]. We obtain

$$W_{\Sigma}^{-1} \circ M = G^{-1}(k + p/2) G^{-1}(k - p/2) [iG(k + \Omega/2) - iG(k - \Omega/2)]. \quad (4.4)$$

$$\tilde{L}_{\text{MT}}[F](k) = -W_{\text{MT}} \circ M[F](k) = g^2 \int \frac{d^3 k'}{(2\pi)^3} D(k - k') [iG(k' + i\Omega/2) - iG(k' - i\Omega/2)] [-F(k')]. \quad (4.5)$$

$$\begin{aligned} \tilde{L}_{\text{AL}}[F](k_1) &= -W_{\text{AL}} \circ M[F](k_1) = g^4 \int \frac{d^3 q d^3 k_2}{(2\pi)^6} G(k_1 - q) (G(k_2 - q) + G(k_2 + q)) D(q + p/2) D(q - p/2) \\ &\times [iG(k_2 + i\Omega/2) - iG(k_2 - i\Omega/2)] F(k_2). \end{aligned} \quad (4.6)$$

The expression for the Maki-Thompson part (4.5)

is identical to the homogeneous limit ($\mathbf{p} = 0$). The

Aslamazov-Larkin part (4.6) is slightly different because the boson propagator pair $D(q+p/2)D(q-p/2)$ knows about the finite CoM momentum. This \mathbf{p} dependence reflects the fact that the boson can also propagate in space. However, within the Eliashberg approximation

the bosons move much slower than the fermions, so we can ignore this effect and assume \tilde{L}_{AL} also coincides with the homogeneous limit. The last part to take care of is Eq.(4.4). We expand it to linear order in \mathbf{p} , and we obtain

$$W_{\Sigma}^{-1} \circ M = \Omega + i\mathbf{v}_k \cdot \mathbf{p} + i\Sigma(i\omega + i\Omega/2) - i\Sigma(i\omega - i\Omega/2) + \delta\mathcal{L}, \quad (4.7)$$

where $\mathbf{v}_k = \nabla_k \xi_k$ and

$$\delta\mathcal{L} = -\frac{i}{2}\mathbf{v}_k \cdot \mathbf{p} \left(\frac{G(i\omega + i\Omega/2, \mathbf{k})}{G(i\omega - i\Omega/2, \mathbf{k})} + \frac{G(i\omega - i\Omega/2, \mathbf{k})}{G(i\omega + i\Omega/2, \mathbf{k})} \right). \quad (4.8)$$

Combining everything together, we obtain

$$\mathcal{L} = \Omega + i\mathbf{v}_k \cdot \mathbf{p} + L_{MT+DOS} + L_{AL} + \delta\mathcal{L}. \quad (4.9)$$

Here the self-energy terms in (4.7) are combined with (4.5) to obtain L_{MT+DOS} , and we approximated \tilde{L}_{AL} by L_{AL} . To access the hydrodynamic regimes, we project the operator (4.9) onto the subspace of soft modes. In [63] we have shown that to leading order the eigenfunc-

tions of the soft modes are functions of θ_k , Ω and \mathbf{p} only (since the projection is local, we suppress the Ω and \mathbf{p} dependence):

$$|F_{\text{soft}}\rangle = F(\theta_k), \quad (4.10)$$

so the projected matrix element will be $\langle H_{\text{soft}}|\mathcal{L}|F_{\text{soft}}\rangle$ where F and H are two soft mode wavefunctions.

Under this projection, $\delta\mathcal{L}$ becomes

$$\begin{aligned} \langle H_{\text{soft}}|\delta\mathcal{L}|F_{\text{soft}}\rangle &= \mathcal{N} \int \frac{d\omega}{2\pi} \frac{d\xi}{2\pi} \int d\theta_k \left(-\frac{i}{2}v_k |\mathbf{p}| \cos\theta_{kp} \right) \left[\frac{G(i\omega + i\Omega/2, \xi)}{G(i\omega - i\Omega/2, \xi)} + \frac{G(i\omega - i\Omega/2, \xi)}{G(i\omega + i\Omega/2, \xi)} \right] \\ &\times [iG(i\omega + i\Omega/2, \xi) - iG(i\omega - i\Omega/2, \xi)] F(\theta_k) H(\theta_k). \end{aligned} \quad (4.11)$$

To leading order, we can approximate $v_k = v_F$, and we perform the ξ -integral by picking up the residues. However, the ξ -residue of the product of the two brackets is zero, so to leading order $\delta\mathcal{L} = 0$ after projection, so the projected operator $\tilde{\mathcal{L}}$ is

$$\tilde{\mathcal{L}} = \Omega + i\mathbf{v}_k \cdot \mathbf{p} + \underbrace{L_{MT+DOS} + L_{AL}}_L. \quad (4.12)$$

After interpreting L as the collision operator, this is

exactly the kernel of the Boltzmann equation.

Therefore, the computation of $\sigma(\mathbf{p})$ reduces to solving the Boltzmann equation $\tilde{\mathcal{L}}F = \text{Drive}$. We expand F into angular harmonics of θ_k :

$$F = \sum_m \frac{e^{im(\theta_k - \theta_p)}}{2\pi} F_m(\Omega, \mathbf{p}). \quad (4.13)$$

Since $e^{im\theta_k}$ diagonalizes L , we have

$$\tilde{\mathcal{L}}[F] = \sum_m \frac{e^{im(\theta_k - \theta_p)}}{2\pi} \left[(\Omega + \lambda_m^{\text{soft}}) F_m(\Omega, \mathbf{p}) + \frac{iv_F |\mathbf{p}|}{2} (F_{m-1}(\Omega, \mathbf{p}) + F_{m+1}(\Omega, \mathbf{p})) \right]. \quad (4.14)$$

Following the same analysis as the FL hydrodynamics [82, 83, 85], the non-local conductivity $\sigma(\mathbf{p})$ and the kinematic viscosity $\nu(\mathbf{p})$ are exactly given by Eqs.(4.1)

and (4.2) respectively, and the effective scattering rate

is given by a continuous fraction formula

$$\Gamma_2(\mathbf{p}) = \gamma_2 + \frac{z^2}{\gamma_3 + \frac{z^2}{\gamma_4 + \dots}}, \quad (4.15)$$

where $z = v_F |\mathbf{p}|/2$ and $\gamma_m = \Omega + \lambda_m^{\text{soft}}$. For the soft eigenvalues to be significant, we should work in the limit $\Omega \ll T$. Again we ignore the effects of boson thermal mass and assume the Ω -scalings of λ_m^{soft} carries over to scaling in T .

For short lengthscales where z becomes larger than the self-energy, Γ_2 is described by the ballistic limit $\Gamma_2 = z$. At longer lengthscales, Γ_2 can enter the hydrodynamic or the tomographic regimes, which we analyze below:

B. Conventional Hydrodynamics Regime

The conventional hydrodynamic regime is the ultimate long-wavelength regime where $\mathbf{p} \rightarrow 0$. In this regime,

$$\Gamma_2 = \Gamma_{\text{hydro}} = \gamma_2, \quad (4.16)$$

and its scalings are summarized in Table. VII.

C. Tomographic Regime

When we go to a shorter length scale $|\mathbf{p}| > p_*$ which will be specified later, we enter into the tomographic regime where all soft modes can propagate and produces an effective scattering rate whose scaling differs from that of each individual eigenvalue.

We follow the analysis in [83, 85] to solve the recurrence equation for the continuous fraction

$$\Gamma_m(\mathbf{p}) = \gamma_m + \frac{z^2}{\gamma_{m+1} + \frac{z^2}{\gamma_{m+2} + \dots}}. \quad (4.17)$$

We assume γ_m oscillates between two functions $\gamma_o(m)$ and $\gamma_e(m)$ when m is odd and even respectively. In [83, 85], it is shown that we can rewrite Eq.(4.17) into a linear recurrence equation in terms of some auxiliary variables u_m , and then we can approximate the recurrence equation by a differential equation for $u_m = u(m)$:

$$u'' - \frac{\gamma'_o}{\gamma_o} u' - \frac{\gamma_o \gamma_e}{4z^2} u = 0, \quad (4.18)$$

where prime means derivative with respect to m . Then Γ_m is obtained from u_m by

$$\Gamma_m = -\frac{2z^2}{\gamma_o} \frac{d \ln u}{dm}. \quad (4.19)$$

The boundary condition for Eq.(4.18) is $\Gamma_m > 0$ when $m \rightarrow \infty$.

In regimes A,B,C and for circular or convex FS, we have $\gamma_e = \gamma m^2$ and $\gamma_o \simeq \gamma' m^6$, and Eq.(4.18) becomes

$$u'' - \frac{6}{m} u' - \frac{\gamma \gamma'}{4z^2} m^8 u = 0. \quad (4.20)$$

The solution can be expressed in terms of Bessel functions

$$u_m = g^{7/10} (I_{7/10}(g) - I_{-7/10}(g)), \quad (4.21)$$

where $g = \frac{m^5 \sqrt{\gamma \gamma'}}{10z}$ and the linear combination is selected to satisfy the boundary condition. The asymptotic behavior of Γ_2 can then be evaluated by expanding in large z , and we obtain

$$\Gamma_2 = \frac{\Gamma\left(\frac{3}{10}\right)}{2^{4/5} 5^{2/5} \Gamma\left(\frac{7}{10}\right)} \frac{\gamma z^{3/5}}{(\gamma \gamma')^{3/10}} - \frac{4\gamma}{3} + \dots \quad (4.22)$$

Therefore, the length scale below which the tomographic transport becomes important is given by

$$z = \frac{|\mathbf{p}| v_F}{2} \gg \sqrt{\gamma \gamma'}, \quad (4.23)$$

where γ, γ' can be read off from Table. V. We can now apply Eq.(4.22) to regimes A,B,C, and the result is summarized in Table. VII as $\Gamma_{\text{tomographic}}^{\text{circular}}$. The result of regime D has been obtained in Refs. [83, 85]. The momentum scaling $\Gamma_2(|\mathbf{p}|) \propto |\mathbf{p}|^{3/5}$ is the consequence of small-angle scattering, which sets a clear difference from the $|\mathbf{p}|^{1/3}$ scaling due to large-angle scattering [83, 85].

We also attempt to extend to the case concave FS, by substituting $\gamma_o = \gamma m^2$ and $\gamma_e = \gamma' m^2$. Because rotation symmetry is broken, the calculation above does not actually apply, but we hope it might provide the correct scaling. Repeating the analysis above for regimes A,B,C, we find the solution of the differential equation is given by

$$u_m = \exp\left(-\frac{\sqrt{\gamma \gamma'}}{6z} m^3\right), \quad (4.24)$$

and

$$\Gamma_2 = \sqrt{\frac{\gamma'}{\gamma}} z. \quad (4.25)$$

This is similar to the ballistic limit where $\Gamma_2 = z$, but the prefactor is renormalized. As for regime D, because the even- m eigenvalue scales the same way as self-energy, we expect the system to directly crossover to the ballistic regime without the tomographic regime.

Regimes	Γ_{hydro}	$\Gamma_{\text{tomographic}}^{\text{Circular}}$	$\Gamma_{\text{tomographic}}^{\text{Concave}}$
A	$\frac{c_f^2 T^{4/3}}{k_F v_F}$	$(\mathbf{p} v_F)^{3/5} (k_F v_F)^{1/5} (c_f T^{2/3})^{1/5}$	$\mathcal{O}(1) \mathbf{p} v_F$
B	$\frac{c_f^2 T^{4/3}}{k_F v_F}$	$(\mathbf{p} v_F)^{3/5} (k_F v_F)^{1/5} c_f^{4/5} T^{-1/15}$	$\mathcal{O}(1) \mathbf{p} v_F$
C	$\frac{m_b^2 c_f T^2}{k_F^2 \omega_{\text{FL}}}$	$(\mathbf{p} v_F)^{3/5} (k_F v_F)^{3/5} c_f'^{2/5} T^{1/5} \omega_{\text{FL}}^{-2/5} (m_b/k_F)^{4/5}$	$\mathcal{O}(1) \mathbf{p} v_F$
D	$\frac{c_f T^2}{\omega_{\text{FL}}}$	$c_f'^{2/3} (v_F \mathbf{p})^{1/3} (k_F v_F)^{1/3} \omega_{\text{FL}}^{-2/3} T$	N.A.

TABLE VII: Scalings of the effective scattering rate Γ_2 defined in (4.2) in the hydrodynamic regime and the tomographic regime. In the hydrodynamic regime, the effective scattering rate equals λ_2^{soft} . For the circular Fermi surface, in the tomographic regime Γ_2 depends on the external wavevector $|\mathbf{p}|$ and scales nontrivially with temperature due to the propagation of the soft modes. For the concave FS, the tomographic regime looks similar to the ballistic regime where $\Gamma_2 \propto |\mathbf{p}|v_F$, but the numerical prefactor can be renormalized.

V. CONCLUSION

In this work, we applied the kinetic operator formalism to study the transport properties of various regimes of the critical Fermi surface, using the Ising-Nematic QCP as an example (see the phase diagram Fig. 1). We obtained the operator spectrum of the critical FS in Sec. II and applied it to optical conductivity in Sec. III. We obtained results for different regimes in the phase diagram (Fig. 1) and different FS geometries as summarized in Tables. IV and VI. In Sec. IV, we applied our formalism to study the hydrodynamics of the critical FS, and we calculated the viscosities and the result is presented in Eqs.(4.1), (4.2) and Table. VII.

Our computation of the optical conductivity, with results agreeing with the recent perturbative calculation [42], also provides a few new perspective to understanding transport:

First, our formalism extends the Prange-Kadanoff reduction formalism [44, 86] into a systematic expansion in $\xi/(k_F v_F)$, and this allows us to perform computation in the NFL regime A.

Second, a natural picture that emerges from our formalism is that the conductivity is a sum of different conduction channels, which are eigenfunctions of the kinetic operator L in the energy and momentum domain. From our results, we believe the usage of extended Drude formula is not appropriate for momentum conserved systems. The textbook Drude formula [87] is derived in the context with momentum relaxation, where the dominant transport lifetime τ is the momentum relaxation time. In a momentum conserved system, momentum cannot contribute to $\text{Re}\sigma(\omega)$ at the leading order, and we found several mechanisms for $\text{Re}\sigma(\omega)$:

1. In the NFL regime A, the overlap between the current and the momentum has non-analytic dependence on $|\omega|$, and this is reflected as a correction to the Drude peak σ_D .

2. For a non-circular FS, the current does not fully overlap with the momentum at zero energy. The remaining part of the current operator is the soft modes of the FS which describe its shape fluctuations. These soft modes lead to a Drude-like contribution σ'_D where the transport lifetime is the inverse eigenvalue of these soft modes.

3. The current also overlaps with other finite-energy channels and they contribute to the incoherent conductivity σ_i . This is an explicit example that invalidates the Drude picture because the overlap between current and these incoherent channels vanishes at zero energy. In previous literature there is a wrong conception that the $\sigma_i \sim T^4 \ln T/\omega^2$ incoherent conductivity in the FL regimes C and D can be interpreted as a scattering rate $\gamma \sim T^4 \ln T$ via the extended Drude formula, and so it was conjectured to be related to the soft-mode scattering rate which also scales as T^4 for a convex, large-angle scattering FL. This interpretation is incorrect because the σ_i can appear for any FS geometry where the T^4 soft-mode scaling does not always apply. The correct interpretation provided by our calculation is that the T^2 factor in σ_i is due to the energy-dependent overlap between the current and the conduction channel, and the transport lifetime of that channel is actually $T^2 \ln T$ which is the natural expectation from self-energy.

Perturbative calculations can in principle obtain the same total conductivity which is the sum of the above mechanisms, but it cannot isolate each individual contributions because perturbative calculations are directly evaluating the inverse of the kinetic operator L , so all eigenvectors are mixed together.

Because the (homogeneous) optical conductivity contains various conduction channels, it is not convenient

as a probe for the critical FS physics. Instead, the non-local conductivity $\sigma(\mathbf{q})$ measured in the hydrodynamics regime is much cleaner in the sense that it is dominated by the propagation of the FS soft modes. Therefore, the viscosities we calculated in Eq.(4.2) and Table. VII are a more direct signature of the NFL physics.

ACKNOWLEDGMENTS

We thank Dmitrii L. Maslov, Andrey V. Chubukov and Alex Levchenko for the inspiring discussions that initiated this work at the KITP program “Quantum Materials With And Without Quasiparticles”. KITP is supported in part by the National Science Foundation under Grants No. NSF PHY-1748958 and PHY-2309135. We thank Debanjan Chowdhury, Zhengyan Darius Shi, Hart Goldman, Senthil Todadri, Leonid Levitov, Jörg Schmalian, Aavishkar A. Patel, Ilya Esterlis and Subir Sachdev for helpful discussions. Haoyu Guo is supported by the Bethe-Wilkins-KIC postdoctoral fellowship at Cornell University.

-
- [1] S.-S. Lee, Recent Developments in Non-Fermi Liquid Theory, *Annual Review of Condensed Matter Physics* **9**, 227 (2018).
- [2] P. A. Lee, Gauge field, Aharonov-Bohm flux, and high- T_c superconductivity, *Phys. Rev. Lett.* **63**, 680 (1989).
- [3] A. J. Millis, Effect of a nonzero temperature on quantum critical points in itinerant fermion systems, *Phys. Rev. B* **48**, 7183 (1993).
- [4] J. Polchinski, Low-energy dynamics of the spinon-gauge system, *Nuclear Physics B* **422**, 617 (1994).
- [5] B. I. Halperin, P. A. Lee, and N. Read, Theory of the half-filled Landau level, *Phys. Rev. B* **47**, 7312 (1993).
- [6] Y. B. Kim, A. Furusaki, X.-G. Wen, and P. A. Lee, Gauge-invariant response functions of fermions coupled to a gauge field, *Phys. Rev. B* **50**, 17917 (1994).
- [7] C. Nayak and F. Wilczek, Renormalization group approach to low temperature properties of a non-Fermi liquid metal, *Nuclear Physics B* **430**, 534 (1994).
- [8] S.-S. Lee, Low-energy effective theory of Fermi surface coupled with U(1) gauge field in $2 + 1$ dimensions, *Phys. Rev. B* **80**, 165102 (2009).
- [9] M. A. Metlitski and S. Sachdev, Quantum phase transitions of metals in two spatial dimensions. I. Ising-nematic order, *Phys. Rev. B* **82**, 075127 (2010).
- [10] D. F. Mross, J. McGreevy, H. Liu, and T. Senthil, Controlled expansion for certain non-Fermi-liquid metals, *Phys. Rev. B* **82**, 045121 (2010).
- [11] S. Sur and S.-S. Lee, Chiral non-Fermi liquids, *Phys. Rev. B* **90**, 045121 (2014).
- [12] M. A. Metlitski, D. F. Mross, S. Sachdev, and T. Senthil, Cooper pairing in non-Fermi liquids, *Phys. Rev. B* **91**, 115111 (2015), arxiv:1403.3694 [cond-mat.str-el].
- [13] S. A. Hartnoll, R. Mahajan, M. Punk, and S. Sachdev, Transport near the Ising-nematic quantum critical point of metals in two dimensions, *Phys. Rev. B* **89**, 155130 (2014).
- [14] A. Eberlein, A. A. Patel, and S. Sachdev, Shear viscosity at the Ising-nematic quantum critical point in two-dimensional metals, *Phys. Rev. B* **95**, 075127 (2017).
- [15] T. Holder and W. Metzner, Anomalous dynamical scaling from nematic and U(1) gauge field fluctuations in two-dimensional metals, *Phys. Rev. B* **92**, 041112 (2015).
- [16] T. Holder and W. Metzner, Fermion loops and improved power-counting in two-dimensional critical metals with singular forward scattering, *Phys. Rev. B* **92**, 245128 (2015).
- [17] A. L. Fitzpatrick, S. Kachru, J. Kaplan, and S. Raghu, Non-Fermi-liquid behavior of large- N_B quantum critical metals, *Phys. Rev. B* **89**, 165114 (2014), arxiv:1312.3321 [cond-mat.str-el].
- [18] J. A. Damia, S. Kachru, S. Raghu, and G. Torroba, Two-Dimensional Non-Fermi-Liquid Metals: A Solvable Large- N Limit, *Phys. Rev. Lett.* **123**, 096402 (2019).
- [19] J. A. Damia, M. Solís, and G. Torroba, How non-Fermi liquids cure their infrared divergences, *Phys. Rev. B* **102**, 045147 (2020).
- [20] J. A. Damia, M. Solís, and G. Torroba, Thermal effects in non-Fermi liquid superconductivity, *Phys. Rev. B* **103**, 155161 (2021).
- [21] S. P. Ridgway and C. A. Hooley, Non-Fermi-Liquid Behavior and Anomalous Suppression of Landau Damping in Layered Metals Close to Ferromagnetism, *Phys. Rev. Lett.* **114**, 226404 (2015).
- [22] A. A. Patel, J. McGreevy, D. P. Arovas, and S. Sachdev, Magnetotransport in a Model of a Disordered Strange Metal, *Phys. Rev. X* **8**, 021049 (2018).
- [23] D. Chowdhury, Y. Werman, E. Berg, and T. Senthil, Translationally invariant non-Fermi liquid metals with critical Fermi-surfaces: Solvable models, *Phys. Rev. X* **8**, 031024 (2018), arxiv:1801.06178 [cond-mat.str-el].
- [24] E.-G. Moon and A. Chubukov, Quantum-critical pairing with varying exponents, *Journal of Low Temperature Physics* **161**, 263 (2010), arxiv:1005.0356 [cond-mat.supr-con].
- [25] A. Abanov and A. V. Chubukov, Interplay between superconductivity and non-Fermi liquid at a quantum critical point in a metal. I., *Phys. Rev. B* **102**, 024524 (2020).
- [26] Y.-M. Wu, A. Abanov, Y. Wang, and A. V. Chubukov, Interplay between superconductivity and non-Fermi liquid at a quantum critical point in a metal. II. The γ model at a finite T for $0 < \gamma < 1$, *Phys. Rev. B* **102**, 024525 (2020), arxiv:2006.02968 [cond-mat.supr-con].

- [27] A. V. Chubukov, A. Abanov, I. Esterlis, and S. A. Kivelson, Eliashberg theory of phonon-mediated superconductivity – when it is valid and how it breaks down, *Annals of Physics* **417**, 168190 (2020), [arxiv:2004.01281 \[cond-mat\]](#).
- [28] X. Wang and E. Berg, Scattering mechanisms and electrical transport near an Ising nematic quantum critical point, *Phys. Rev. B* **99**, 235136 (2019), [arxiv:1902.04590 \[cond-mat.str-el\]](#).
- [29] A. Klein, A. V. Chubukov, Y. Schattner, and E. Berg, Normal State Properties of Quantum Critical Metals at Finite Temperature, *Phys. Rev. X* **10**, 031053 (2020).
- [30] O. Grossman, J. S. Hofmann, T. Holder, and E. Berg, Specific heat of a quantum critical metal, *Physical Review Letters* **127**, 10.1103/physrevlett.127.017601 (2021).
- [31] D. Chowdhury and E. Berg, The unreasonable effectiveness of Eliashberg theory for pairing of non-Fermi liquids, *Annals of Physics* **417**, 168125 (2020), [arxiv:1912.07646 \[cond-mat.supr-con\]](#).
- [32] I. Esterlis and J. Schmalian, Cooper pairing of incoherent electrons: An electron-phonon version of the Sachdev-Ye-Kitaev model, *Phys. Rev. B* **100**, 115132 (2019), [arxiv:1906.04747 \[cond-mat.str-el\]](#).
- [33] D. Hauck, M. J. Klug, I. Esterlis, and J. Schmalian, Eliashberg equations for an electron-phonon version of the Sachdev-Ye-Kitaev model: Pair breaking in non-Fermi liquid superconductors, *Annals of Physics* **417**, 168120 (2020), [arxiv:1911.04328 \[cond-mat.str-el\]](#).
- [34] Y. Wang and A. V. Chubukov, Quantum phase transition in the yukawa-SYK model, *Phys. Rev. Res.* **2**, 033084 (2020), [arxiv:2005.07205 \[cond-mat.str-el\]](#).
- [35] E. E. Aldape, T. Cookmeyer, A. A. Patel, and E. Altman, Solvable theory of a strange metal at the breakdown of a heavy Fermi liquid, *Phys. Rev. B* **105**, 235111 (2022), [arxiv:2012.00763 \[cond-mat.str-el\]](#).
- [36] A. A. Patel and S. Sachdev, Quantum chaos on a critical Fermi surface, *Proc. Nat. Acad. Sci.* **114**, 1844 (2017), [arxiv:1611.00003 \[cond-mat.str-el\]](#).
- [37] A. A. Patel and S. Sachdev, Theory of a planckian metal, *Physical Review Letters* **123**, 10.1103/physrevlett.123.066601 (2019).
- [38] V. Oganesyan, S. A. Kivelson, and E. Fradkin, Quantum theory of a nematic Fermi fluid, *Phys. Rev. B* **64**, 195109 (2001).
- [39] A. A. Patel and S. Sachdev, Critical strange metal from fluctuating gauge fields in a solvable random model, *Phys. Rev. B* **98**, 125134 (2018), [arxiv:1807.04754 \[cond-mat.str-el\]](#).
- [40] A. V. Chubukov and D. L. Maslov, Optical conductivity of a two-dimensional metal near a quantum critical point: The status of the extended Drude formula, *Phys. Rev. B* **96**, 205136 (2017), [arxiv:1707.07352 \[cond-mat.str-el\]](#).
- [41] D. L. Maslov and A. V. Chubukov, Optical response of correlated electron systems, *Reports on Progress in Physics* **80**, 026503 (2017), [arxiv:1608.02514 \[cond-mat.str-el\]](#).
- [42] S. Li, P. Sharma, A. Levchenko, and D. L. Maslov, Optical conductivity of a metal near an Ising-nematic quantum critical point (2023), [arxiv:2309.12571 \[cond-mat\]](#).
- [43] I. Esterlis, H. Guo, A. A. Patel, and S. Sachdev, Large N theory of critical Fermi surfaces, *Phys. Rev. B* **103**, 235129 (2021), [arxiv:2103.08615 \[cond-mat.str-el\]](#).
- [44] H. Guo, A. A. Patel, I. Esterlis, and S. Sachdev, Large N theory of critical Fermi surfaces II: Conductivity, *Phys. Rev. B* **106**, 115151 (2022), [arxiv:2207.08841 \[cond-mat, physics.hep-th\]](#).
- [45] H. Guo, D. Valentinis, J. Schmalian, S. Sachdev, and A. A. Patel, Cyclotron resonance and quantum oscillations of critical Fermi surfaces (2023), [arxiv:2308.01956 \[cond-mat\]](#).
- [46] L. V. Delacrétaz, Y.-H. Du, U. Mehta, and D. T. Son, Nonlinear bosonization of Fermi surfaces: The method of coadjoint orbits, *Phys. Rev. Res.* **4**, 033131 (2022).
- [47] S. Han, F. Desrochers, and Y. B. Kim, Bosonization of Non-Fermi Liquids (2023), [arxiv:2306.14955 \[cond-mat, physics.hep-th\]](#).
- [48] U. Mehta, Postmodern Fermi Liquids (2023), [arxiv:2307.02536 \[cond-mat, physics.hep-th\]](#).
- [49] D. V. Else, R. Thorngren, and T. Senthil, Non-fermi liquids as ersatz fermi liquids: General constraints on compressible metals, *Physical Review X* **11**, 10.1103/physrevx.11.021005 (2021).
- [50] D. V. Else and T. Senthil, Critical drag as a mechanism for resistivity, *Phys. Rev. B* **104**, 205132 (2021), [arxiv:2106.15623 \[cond-mat.str-el\]](#).
- [51] Z. D. Shi, H. Goldman, D. V. Else, and T. Senthil, Gifts from anomalies: Exact results for Landau phase transitions in metals, *SciPost Physics* **13**, 102 (2022).
- [52] Z. D. Shi, D. V. Else, H. Goldman, and T. Senthil, Loop current fluctuations and quantum critical transport, *SciPost Physics* **14**, 113 (2023).
- [53] T. Park and L. Balents, An exact method for bosonizing the Fermi surface in arbitrary dimensions (2023), [arxiv:2310.04636 \[cond-mat\]](#).
- [54] D. Chowdhury, A. Georges, O. Parcollet, and S. Sachdev, Sachdev-Ye-Kitaev models and beyond: Window into non-Fermi liquids, *Reviews of Modern Physics* **94**, 10.1103/revmodphys.94.035004 (2022).
- [55] A. A. Patel, H. Guo, I. Esterlis, and S. Sachdev, Universal theory of strange metals from spatially random interactions, *Science* **381**, 790 (2023).
- [56] F. Marsiglio, Eliashberg theory: A short review, *Annals of Physics Eliashberg Theory at 60: Strong-coupling Superconductivity and Beyond*, **417**, 168102 (2020).
- [57] W. Kohn, Cyclotron Resonance and de Haas-van Alphen Oscillations of an Interacting Electron Gas, *Phys. Rev.* **123**, 1242 (1961).
- [58] D. L. Maslov, V. I. Yudson, and A. V. Chubukov, Resistivity of a Non-Galilean-Invariant Fermi Liquid near Pomeranchuk Quantum Criticality, *Phys. Rev. Lett.* **106**, 106403 (2011).
- [59] H. K. Pal, V. I. Yudson, and D. L. Maslov, Resistivity of non-Galilean-invariant Fermi- and non-Fermi liquids, *Lithuanian Journal of Physics* **52**, 10.3952/physics.v52i2.2358 (2012).
- [60] P. B. Allen, Electron-Phonon Effects in the Infrared Properties of Metals, *Phys. Rev. B* **3**, 305 (1971).
- [61] J. W. Allen and J. C. Mikkelsen, Optical properties of CrSb, MnSb, NiSb, and NiAs, *Phys. Rev. B* **15**, 2952 (1977).
- [62] N. P. Armitage, Electrodynamics of correlated electron systems (2018), [arxiv:0908.1126 \[cond-mat\]](#).

- [63] H. Guo, Is the migdal-eliasberg theory for 2+1d critical fermi surface stable? (2023), [arXiv:2311.03455](https://arxiv.org/abs/2311.03455) [cond-mat.str-el].
- [64] R. N. Gurzhi, Reviews of Topical Problems: Hydrodynamic Effects in Solids at Low Temperature, *Soviet Physics Uspekhi* **11**, 255 (1968).
- [65] R. Jaggi, Electron-fluid model for dc size effect, *Journal of Applied Physics* **69**, 816 (1991).
- [66] M. J. M. de Jong and L. W. Molenkamp, Hydrodynamic electron flow in high-mobility wires, *Phys. Rev. B* **51**, 13389 (1995).
- [67] M. Mueller and S. Sachdev, Collective cyclotron motion of the relativistic plasma in graphene, *Phys. Rev. B* **78**, 115419 (2008), [arxiv:0801.2970](https://arxiv.org/abs/0801.2970) [cond-mat, physics:hep-th].
- [68] M. Müller, J. Schmalian, and L. Fritz, Graphene: A Nearly Perfect Fluid, *Phys. Rev. Lett.* **103**, 025301 (2009).
- [69] A. V. Andreev, S. A. Kivelson, and B. Spivak, Hydrodynamic Description of Transport in Strongly Correlated Electron Systems, *Phys. Rev. Lett.* **106**, 256804 (2011).
- [70] A. Lucas, J. Crossno, K. C. Fong, P. Kim, and S. Sachdev, Transport in inhomogeneous quantum critical fluids and in the Dirac fluid in graphene, *Phys. Rev. B* **93**, 075426 (2016).
- [71] B. N. Narozhny, I. V. Gornyi, M. Titov, M. Schütt, and A. D. Mirlin, Hydrodynamics in graphene: Linear-response transport, *Phys. Rev. B* **91**, 035414 (2015).
- [72] A. Principi, G. Vignale, M. Carrega, and M. Polini, Bulk and shear viscosities of the two-dimensional electron liquid in a doped graphene sheet, *Phys. Rev. B* **93**, 125410 (2016).
- [73] L. Levitov and G. Falkovich, Electron viscosity, current vortices and negative nonlocal resistance in graphene, *Nature Phys* **12**, 672 (2016).
- [74] G. Falkovich and L. Levitov, Linking Spatial Distributions of Potential and Current in Viscous Electronics, *Phys. Rev. Lett.* **119**, 066601 (2017).
- [75] D. A. Bandurin, I. Torre, R. K. Kumar, M. Ben Shalom, A. Tomadin, A. Principi, G. H. Auton, E. Khestanova, K. S. Novoselov, I. V. Grigorieva, L. A. Ponomarenko, A. K. Geim, and M. Polini, Negative local resistance caused by viscous electron backflow in graphene, *Science* **351**, 1055 (2016).
- [76] J. Crossno, J. K. Shi, K. Wang, X. Liu, A. Harzheim, A. Lucas, S. Sachdev, P. Kim, T. Taniguchi, K. Watanabe, T. A. Ohki, and K. C. Fong, Observation of the Dirac fluid and the breakdown of the Wiedemann-Franz law in graphene, *Science* **351**, 1058 (2016), [arxiv:1509.04713](https://arxiv.org/abs/1509.04713) [cond-mat.mes-hall].
- [77] L. V. Delacretaz, *Hydrodynamics of Condensed Matter*, Ph.D. thesis, Stanford University, United States – California (2019).
- [78] H. Guo, E. Ilseven, G. Falkovich, and L. Levitov, *Stokes Paradox, Back Reflections and Interaction-Enhanced Conduction* (2017), [arxiv:1612.09239](https://arxiv.org/abs/1612.09239) [cond-mat].
- [79] H. Guo, E. Ilseven, G. Falkovich, and L. S. Levitov, Higher-than-ballistic conduction of viscous electron flows, *Proceedings of the National Academy of Sciences* **114**, 3068 (2017).
- [80] H. Guo, *Signatures of Hydrodynamic Transport in an Electron System*, Thesis, Massachusetts Institute of Technology (2018).
- [81] R. Krishna Kumar, D. A. Bandurin, F. M. D. Pellegrino, Y. Cao, A. Principi, H. Guo, G. H. Auton, M. Ben Shalom, L. A. Ponomarenko, G. Falkovich, K. Watanabe, T. Taniguchi, I. V. Grigorieva, L. S. Levitov, M. Polini, and A. K. Geim, Superballistic flow of viscous electron fluid through graphene constrictions, *Nature Phys* **13**, 1182 (2017).
- [82] P. Ledwith, H. Guo, A. Shytov, and L. Levitov, Tomographic Dynamics and Scale-Dependent Viscosity in 2D Electron Systems, *Phys. Rev. Lett.* **123**, 116601 (2019).
- [83] S. Kryhin, Q. Hong, and L. Levitov, *T*-linear conductance in electron hydrodynamics (2023), [arxiv:2310.08556](https://arxiv.org/abs/2310.08556) [cond-mat].
- [84] P. J. Ledwith, H. Guo, and L. Levitov, The hierarchy of excitation lifetimes in two-dimensional Fermi gases, *Annals of Physics* **411**, 167913 (2019).
- [85] Q. Hong, M. Davydova, P. J. Ledwith, and L. Levitov, *Superscreening by a Retroreflected Hole Backflow in Tomographic Electron Fluids* (2020), [arxiv:2012.03840](https://arxiv.org/abs/2012.03840) [cond-mat].
- [86] R. E. Prange and L. P. Kadanoff, Transport theory for electron-phonon interactions in metals, *Phys. Rev.* **134**, A566 (1964).
- [87] N. W. Ashcroft, *Solid State Physics* (Holt, Rinehart and Winston, New York, 1976).